A Study on Venlafaxine HCL with Dendrimer, DNA, RNA and BSA, Silver Nanoparticles: Spectral and Molecular Docking Methods

Narayanasamy Rajendiran[1*], Ayyadurai Mani[1], Poomalai Senthilraja[2], S. Senthilmurugan[3]

[1]Department of Chemistry, Annamalai University, Annamalai Nagar, Tamilnadu, India

[2]Department of Bioinformatics, Bharathidasan University, Tiruchy, Tamilnadu, India

[3]Department of Zoology, Annamalai University, Annamalai Nagar, Tamilnadu, India

***Corresponding Author**

DOI: https://doi.org/10.51244/IJRSI.2026.1303000213

Received: 31 March 2026; Accepted: 06 April 2026; Published: 17 April 2026

ABSTRACT

The absorption, emission, and molecular docking characteristics of venlafaxine hydrochloride (VF) were investigated in the presence of various biomolecular systems (PAMAM-OH dendrimers, DNA, RNA, BSA) and silver nanoparticles (AgNPs). Upon interaction with these biomolecules, the characteristic absorption and emission maxima of VF were significantly quenched or completely diminished. The negative calculated values of the free energies suggest that the binding processes between VF and the biomolecules are spontaneous. VF exhibited stronger binding affinity to DNA in the ground state, whereas its interaction with RNA was more pronounced in the excited state. The binding mechanisms were predominantly governed by intercalative interactions, van der Waals forces, and hydrogen bonding. The addition of VF-biomolecule complexes to AgNPs resulted in either red or blue shifts in the optical spectra, reflecting changes in the electronic environment and binding dynamics. Molecular docking studies revealed specific interactions between the nitrogen, oxygen, and hydrogen atoms of VF and the biomolecular targets. Additionally, VF demonstrated potential anticancer activity through strong binding affinities with EGFR protein targets, specifically 1r51 and 2oh4, supporting its relevance in cancer therapeutics.

Keywords: Dendrimer, DNA, RNA, BSA, Venlafaxine, Ag Nanoparticles, Anticancer

INTRODUCTION

The interaction between nanoparticles (NPs) and proteins underpins several emerging strategies in the self-assembly of nanostructures and has broad implications in nanotechnology applications [1–11]. Upon introduction into biological systems, such as tissues or fluids like blood, NPs often undergo spontaneous interactions with surrounding proteins. This results in the formation of a molecular layer known as the *protein corona*, which adsorbs onto the NP surface and significantly alters its biological identity and behavior. Understanding the physicochemical characteristics of NP–protein corona interactions is essential for assessing their impact on protein function, biodistribution, and potential toxicity [12].

Nanoparticles are widely utilized in biomedical and clinical contexts due to their unique physical and chemical properties. These include size and shape tunability, straightforward characterization via UV–V is spectroscopy and electron microscopy, immune evasion potential, and distinctive optical features such as surface plasmon resonance (SPR), which can enhance fluorescence signals. Chemically, NPs offer high stability, low cytotoxicity, and strong selectivity, enabling specific and efficient interactions with biomolecular targets [13,14].

Hence, in this study, we selected a biological macromolecule (PAMAM-OH dendrimers, deoxyribonucleic acid (DNA), ribonucleic acid (RNA), and bovine serum albumin (BSA)) for analysis. These biomolecules are prevalent in blood plasma and commonly comprise the corona surrounding various nanoparticles [15,16]. Molecular docking simulations, a powerful computational tool for modeling interactions at the atomic and molecular levels, were employed to predict the optimal binding conformations of these biomolecules with drug, and to investigate the nature of the resulting interactions [11,17,18].

Previous studies have extensively examined the interactions between drugs, nanoparticles, and biomolecules using spectroscopic methods such as UV-visible and fluorescence spectroscopy [19–22]. Based on the above, we investigated the photophysical behavior of VF in the presence of PAMAM-OH dendrimers, DNA, RNA, BSA, and silver nanoparticles (AgNPs) using both experimental spectroscopic techniques and molecular docking approaches. Further, the anticancer potential of VF was evaluated via in silico docking against key epidermal growth factor receptor (EGFR) protein targets.

Venlafaxine hydrochloride (**VF,** 1-[2-(dimethylamino)-1-(4-methoxyphenyl) ethyl] cyclohexan-1-ol hydrochloride) is a widely prescribed antidepressant used in the treatment of major depressive disorder, generalized anxiety disorder, panic disorder, and social anxiety disorder. While generally well-tolerated, VF can induce side effects such as hyperhidrosis, dry mouth, nausea, somnolence, dizziness, and sexual dysfunction, including erectile difficulties and delayed ejaculation. The chemical structure of VF is shown in Figure 1.

Experimental

Preparation of Drug:Biomolecule solution

Standard solutions containing biomolecules such as PAMAM-OH dendrimer, DNA, RNA, or BSA at a concentration of 1.0×10^{-4} M were prepared in varying volumes (0.1–1.0 mL) in 10 mL volumetric flasks. To each flask, 0.2 mL of a 2×10^{-2} M VF solution was added. The mixtures were thoroughly homogenized and diluted to a final volume of 10 mL with triple-distilled water, resulting in a uniform final VF concentration of 4×10^{-4} M in all solutions.

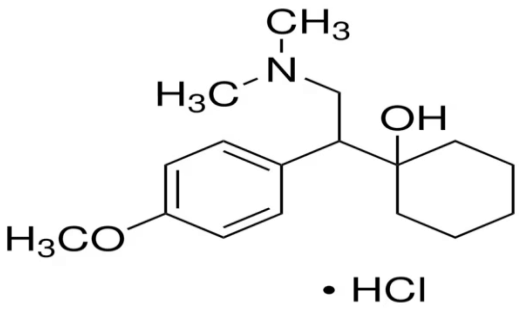

Fig.1. Chemical structure of venlafaxine HCl

Preparation of Silver and Ag/VF/Biomolecule Nanoparticles

Silver nanoparticles were synthesized by dissolving 0.01 M silver nitrate in 200 mL of deionized water, followed by heating the solution at 50–60 °C for 30 minutes. While maintaining vigorous stirring, 1–2 mL of a 1% trisodium citrate solution (prepared by dissolving 1 g of trisodium citrate in 100 mL of deionized water) was added dropwise. The successful formation of silver nanoparticles was indicated by the development of a pale-yellow color, consistent with previous reports [19–22].

To prepare the Ag/VF/biomolecule complex, VF (2×10^{-3} M in 20 mL ethanol) was slowly introduced into the biomolecule solution (2×10^{-4} M in 80 mL deionized water) under constant stirring. The resulting mixture was heated to 50 °C and stirred continuously for 2 hours using a magnetic stirrer. Subsequently, 50 mL of the prepared silver nanoparticle solution (0.01 M) was combined with 50 mL of the VF/biomolecule solution, and the mixture was further stirred for an additional 2 hours [19–22].

ISSN No. 2321-2705 | DOI: 10.51244/IJRSI |Volume XIII Issue III March 2026

Molecular docking method

AutoDock molecular docking software suite that integrates methodologies such as simulated annealing, local gradient search, and genetic algorithms to predict ligand-receptor interactions [23–28]. Version 4.2.6 of AutoDock is distributed freely under the GNU General Public License (GPL) and is available for Linux, macOS, and Windows platforms via the official website (http://autodock.scripps.edu). In this tools, both AutoDock 4.2.6 and AutoDock Vina are frequently employed in molecular docking research. In this study, molecular docking simulations were conducted using the Lamarckian Genetic Algorithm (LGA) in conjunction with the Solis and Wets local search method. The initial conformations of the ligands, including position, orientation, and torsional angles, were randomly assigned. Each docking experiment consisted of 10 independent runs, with a maximum of 2.5×10^5 energy evaluations per run. A population size of 150 was maintained throughout the simulations. The docking protocol utilized a translational step size of 0.2 Å, while the rotational and torsional step sizes were set to 5° [26–28].

Anticancer Potential of venlafaxine HCl

Molecular docking technique is used to study the intermolecular interactions and binding modes between a drug molecule and a biomolecule. In this process, the macromolecule serves as the protein receptor, while the micromolecule acts as the ligand. The docking analysis was conducted using the licensed software Dassault Systèmes BIOVIA Discovery Studio version 22.1.100. The three-dimensional (3D) structure of the target protein, the Epidermal Growth Factor Receptor (EGFR) complexed with epiregulin (EREG), was obtained from the Protein Data Bank (PDB ID: 5WB7) via https://www.rcsb.org/. Protein preparation involved the removal of water molecules and ions, the addition of hydrogen atoms, and grid setup to identify optimal binding sites. Docking simulations were then performed to analyze the interaction between the ligand and the receptor.

RESULTS AND DISCUSSION

Effect of Venlafaxine HCl on Biomolecules

Absorption and emission spectral maxima of venlafaxine HCl (VF) drug was measured in different concentrations of biomolecules [PAMAM-OH (Dendrimer), DNA, RNA, BSA] and the relevant data is given in Table 1, Fig. 2. In water, the absorption maxima of VF were appearing at 273, 224 nm and the emission maximum appeared at 301 nm. In aqueous solution of the isolated DNA, a single absorption maximum was appearing at 260 nm while three emission maxima noticed at 467, 357 and 320 nm. With increasing the DNA concentrations in VF: a) the absorption maxima were red shifted to 276, 229 nm and the absorbance decreased (Fig. 2), b) the triple emission maxima of the DNA were lost, while emission of VF was noticed at 303 nm and the emission intensity increased.

In aqueous isolated PAMAM-OH solution exhibited a characteristic absorption maximum at 282 nm, along with three distinct emission maxima noted at 300, 355, and 440 nm. Upon increasing the concentration of PAMAM-OH in the presence of VF, (a) no significant shift in the absorption maximum was observed, although a decrease in absorbance was noted, and (b) the original triple emission peaks of PAMAM-OH disappeared, giving rise to a single emission maximum at 302 nm with a concurrent reduction in emission intensity at this wavelength.

Table 1. Absorption and fluorescence maxima of venlafaxine HCl [0.2 x 10^{-4} M] with different PAMAM-OH-Dendrimer, DNA, RNA and BSA concentrations [x10^{-6} M].

Concentration of Biomolecules (M)	**PAMAM-OH-Dendrimer**			**DNA**			**RNA**			**BSA**		
	□abs	log □	□flu	□abs	log □	□flu	□abs	log □	□flu	□abs	log □	□flu
VF only	273 224	2.76 3.99	301	273 224	2.76 3.99	301	273 224	2.76 3.99	301	273 224	2.76 3.99	301

ISSN No. 2321-2705 | DOI: 10.51244/IJRSI |Volume XIII Issue III March 2026

0.2	272 224	2.62 3.91	302	276 224	2.89 3.98	303	273 224	2.72 3.95	308	272	2.67	336
1.0	272 229	2.32 3.50	302	276 229	3.35 3.58	303	273 228	2.49 3.68	308	272	2.42	336
Excitation wavelength (nm)	-	-	270	-	-	270	-	-	270	-	-	270
K (1:1) x10^5 M^{-1}	313	-	227	57	-	120	101	-	74	205	-	512
□G (kcalmol^{-1})	-14.48	-	-13.67	-10.22	-	-12.07	-11.62	-	-10.86	-13.41	-	-15.72

Table 2. Venlafaxine HCl with PAMAM-OH-Dendrimer, DNA, RNA and BSA interaction values.

Protein	Binding energy ΔGb (kcal/ mol)	Intermolec. Energy kcal/mol	Torsional energy	Total Internal energy	Inhibition constant (Ki) (uM)	vdW + H bond + desolv Energy kcal/mol	Electro static Energy kcal/mol	Ligand efficiency	Unbond energy	refRMS
PAMAM	3.59	5.38	1.79	1.06	2.32	5.03	0.36	0.18	1.06	69.74
DNA	7.55	9.34	1.79	0.93	2.92	7.97	1.37	0.38	0.93	26.93
RNA	7.06	8.85	1.79	1.0	6.69	7.14	1.71	0.35	1.0	32.42
BSA	4.68	6.47	1.79	0.83	369.12	5.32	1.15	0.23	0.83	52.03

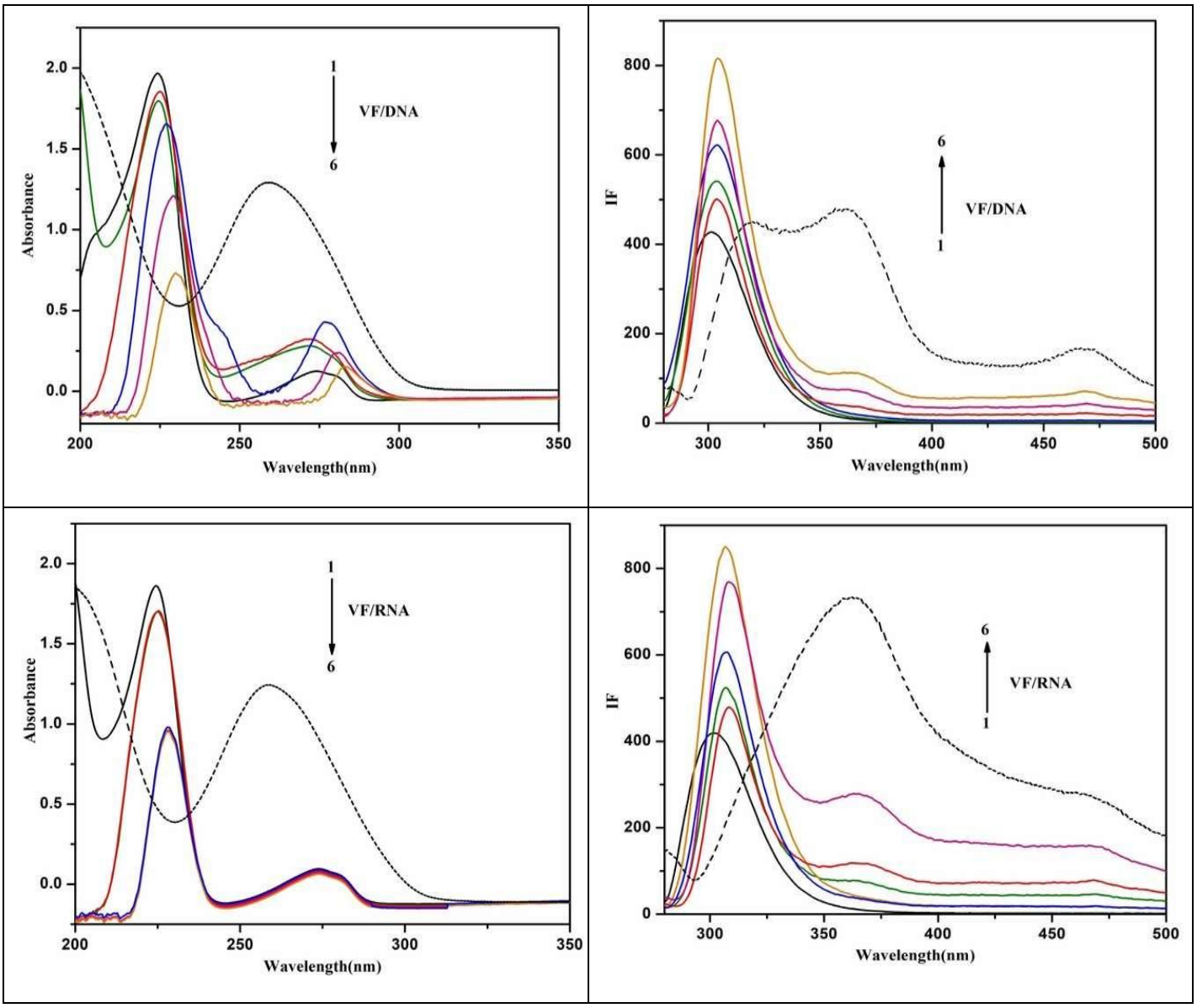

ISSN No. 2321-2705 | DOI: 10.51244/IJRSI |Volume XIII Issue III March 2026

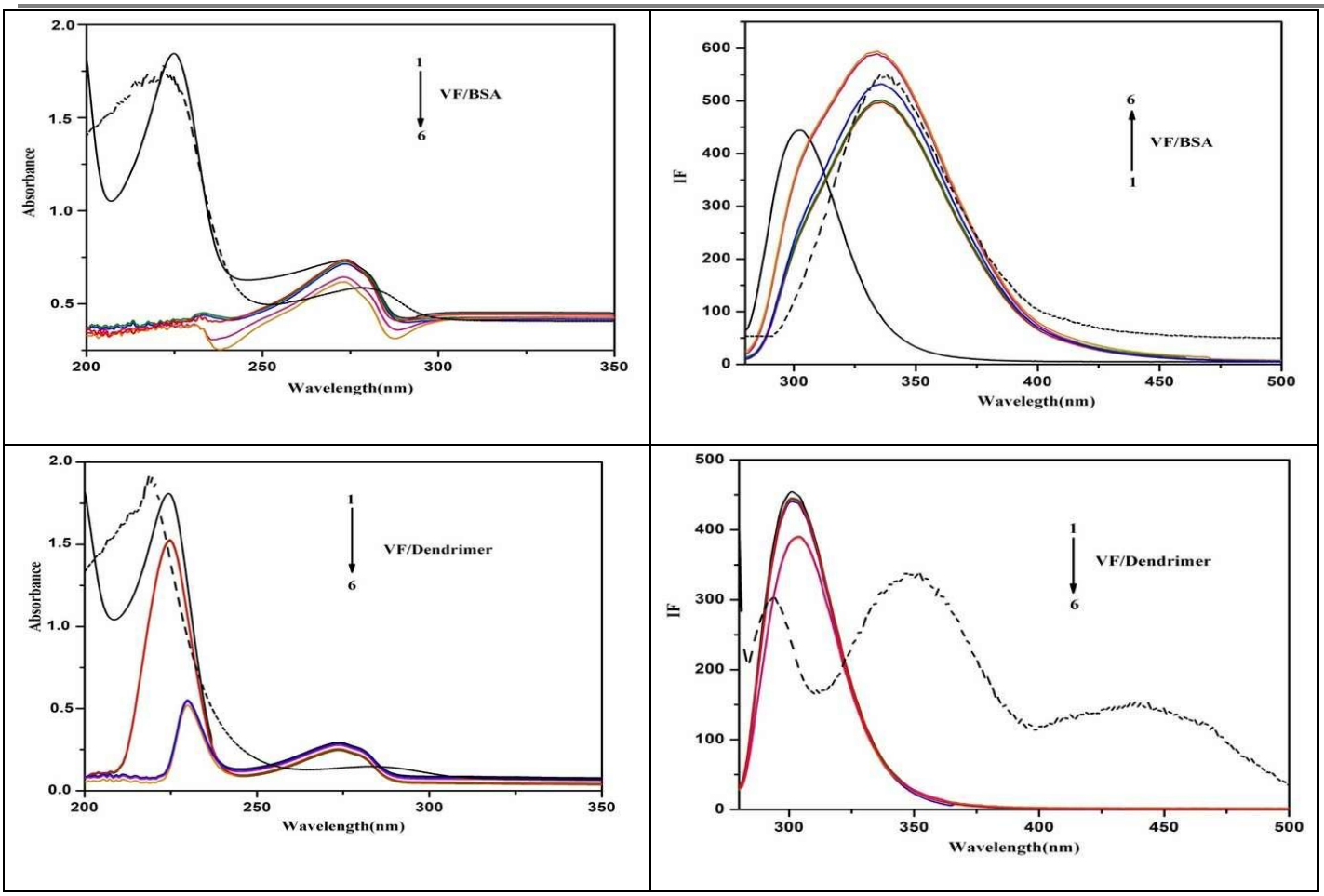

Fig.2. Absorption and fluorescence spectra of venlafaxine HCl [0.2 x10^{-4} M) with different concentrations of biomolecules (DNA, RNA, BSA, Dendrimer) (M x 10^{-6}): 1) 0, 2) 2, 3) 4, 4) 6, 5) 8, 6) 10, dotted line indicates pure biomolecules spectra.

A single absorption maximum was appearing at 258 nm while dual emission was noticed at 362 and 463 nm in aqueous isolated RNA solution. When increasing the RNA concentrations with VF: a) no significant shift was noticed in the absorption maxima and the absorbance decreased at 273, 224 nm, b) a single emission noticed at 308 nm, c) both the shorter and the longer wavelengths of the RNA emission was lost whereas the emission of VF red shifted to 308 nm, and the emission intensity increased.

In aqueous isolated BSA solution, a single absorption and emission maximum was appearing at 278 nm and 336 nm respectively. As the BSA concentrations increased with VF: a) no significant shift noticed in the absorption spectrum and the absorbance decreased, b) a single emission was noticed at 336 nm and the emission maximum of the isolated BSA was lost, c) the emission maximum of the VF was red shifted from 301 to 336 nm and the emission intensity increased.

The absorption and emission results indicating that VF was interacted to all the biomolecules. The skeleton structure of the biomolecules restricts the free rotation of the drug molecule; hence, the absorption and emission intensities of the VF was changed in the biomolecule solution [29-38]. Fig.2 reveals that, in the ground state, drug sensing behaviour of DNA is higher than BSA RNA and PAMAM-OH whereas in the excited state, DNA and BSA is higher than other biomolecules.

The binding strength of the drugs with biomolecules is mirrored in the intrinsic binding constant K, which represents the binding constant per DNA, RNA base pair and per BSA amino acids. It can be obtained by monitoring the changes in the corresponding absorption wavelength with increasing the concentrations of the biomolecules. From the slop and intercept of the Benesi-Hildebrand plot, the binding constant (K) and stoichiometry ratio of the drug with the biomolecule interactions were calculated. The presence of an isosbestic point in the absorption spectra and the above plot confirms the formation of a 1:1 complex. Further, the plot of

ISSN No. 2321-2705 | DOI: 10.51244/IJRSI |Volume XIII Issue III March 2026

$1/(A-A_0)$ versus $1/[Biomolecules]^2$ and $1/(I-I_0)$ vs. $1/[Biomolecules]^2$ gives the concave line suggest 1:2 complex is not formed [29-38]. The characteristic red and blue shift and also sharp isosbestic points indicated clearly the equilibrium in binding phenomenon in all the cases. The negative free energy change (ΔG) values (Table 1), reveal that the binding process was spontaneous and thermodynamically stable at the experimental temperature. The negative Δ*G* value indicated the spontaneity of the sensing between drug and biomolecules. ΔG for VF-BSA is more negative than other biomolecules indicated that its sensing behavior is more spontaneous. The change in free energy of VF-BSA is -15.72 kcal mol^{-1}, this also conform the sensing is higher than that of other drug-biomolecule interactions.

Drug–biomolecule interactions can be studied by comparison of absorption and emission spectra of the free drug, free PAMAM-OH, DNA, RNA, BSA, and drug–biomolecule complexes, which are generally altered. Upon addition of VF drug to the biomolecules, the absorption and emission maxima of the biomolecules are completely disappeared or changed. The absorption and emission maxima of the VF drug is typical results in hyperchromism or hypochromism, hypsochromism (blue shift) and bathochromism (red shift). The gradual change in the absorbance or the emission intensity with the addition of drug to the biomolecules was the sensing of the drug molecules with the biomolecules resulting in formation of drug: biomolecule complex. The spectral shifts showed that different functional groups are interacted with the biomolecules. The obtained results indicated that it is possible to design the structure of these drug-biomolecule complexes by appropriately selecting type, length and functional substituent group in the drug.

Because of the intercalative mode involving a stacking interaction between the drug and the base pair of biomolecules, the extent of the blue shift is consistent with the strength of intercalative interaction [39]. The power of this electronic interaction is expected to decrease as the cube of the distance between the drug and the biomolecule base reduces. By decreasing the distance between the drug and biomolecules, spectral shift takes place apparently. Thus, this is reliable with the combination of π-π electrons of the drug and the DNA bases. Subsequently, the energy level of the π–π-electron transition decreases, which causes a red or blue shift [40, 41]. In case of electrostatic interaction between the drug and the biomolecule, red or blue shift is observed. This reflects some changes in biomolecule conformation and structure after drug–biomolecule interaction is complete. The red or blue shift is increase in absorbance of DNA upon denaturation. The two strands of DNA are held together mainly by the stacking interactions, hydrogen bonds and hydrophobic effect between the complementary bases. The hydrogen bond limits the resonance of the aromatic ring so the absorbance of the sample is limited as well. When the DNA double helix is treated with denaturing agents, the interaction force holding the double helical structure is disturbed. The double helix then separates into two single strands which are in the random coiled conformation. At the moment, the base–base interaction gets reduced, increasing the absorption and emission intensities of biomolecule solution because many bases are in free form and do not form hydrogen bonds with corresponding bases. Red or blue shift reveal the subsequent changes of biomolecule in its conformation and structure after the drug–biomolecule interaction is completed. Further, the blue shift arises mainly due to the presence of charged cations which bind to biomolecule via electrostatic interaction to the phosphate group of DNA backbone and thereby causing a reduction and overall damage to the secondary structure of DNA [42]. The blue shift may also be attributed to external contact (electrostatic binding) [43] or to partial uncoiling of the helix structure of DNA, exposing more bases of the DNA [44]. If there is a weaker interaction, then only hypochromic or blue shifts are observed without significant changes of shifts in the spectral profiles [45].

The slight red shift can best be described by the decrease in π-π transition energy of the drugs due to their ordered stacking between the DNA base pairs after intercalation. After binding to the biomolecules, the π-orbital of the binding drug could pair with π- orbital of base pairs in the biomolecules. The coupling π- orbital is generally partially filled by electrons, thus decreasing the transition probabilities, and hence resulting in the blue shift. The compression in the structure of either the drug alone and/or DNA after the formation of drug–biomolecules complex can result in blue shift [46].

As discussed above, the several changes observed in the absorption and emission spectra indicated that the drugs have interacted with PAMAM-OH, DNA, RNA and BSA. This kind of sensing might have caused the slight change in the conformation of drugs. The absorption and emission intensity of these solutions showed moderate shifts towards the wavelength confirmed that the addition of biomolecule is sensing with the drug.

ISSN No. 2321-2705 | DOI: 10.51244/IJRSI |Volume XIII Issue III March 2026

Formation of Ag/VF/Biomolecules nanoparticle

The absorption and emission spectra of VF, Ag, Ag/VF, Ag/Dendrimer, Ag/DNA, Ag/RNA, Ag/BSA, Ag/VF/Dendrimer, Ag/VF/DNA, Ag/VF/RNA, and Ag/VF/BSA nanoparticles are also investigated. Ag nanoparticle's absorption and emission bond appears at 420, 250 nm and 474, 352 nm respectively. Further, the yellow color was identified for the formation of Ag nanoparticles. Due to surface plasmon resonance, it is known that Ag nanoparticles exhibit their highest absorption in the 400–500 nm range [47-53].

An addition of VF solution to the Ag nano, the absorption maxima blue shifted from 420, 250 nm to 409, 265 nm and emission maxima blue shifted from 474, 352 nm to 467 and 305 nm. When PAMAM-OH added to the Ag nano solution, the absorption maxima red shifted to 427, 280 nm and emission maxima moved to 330, 302 nm respectively. Upon addition of VF/PAMAM-OH solution to the Ag nanoparticles, the absorption and emission maxima red shifted to 426, 274 nm and 505, 307 nm respectively.

By adding DNA solution to the Ag nanoparticles, the absorption maxima red shifted to 436, 262 nm and the emission maxima blue shifted to 470, 423, 362 nm. Gradual addition of VF/DNA solution to the Ag nanoparticles, the absorption and emission maxima blue shifted to 368, 268 nm and 468, 311 nm respectively. With an addition of RNA to the Ag nano solution, the absorption and emission maxima shifted to 445, 260 nm and 364, 325 nm respectively. When VF/RNA solution added to the Ag nanoparticles, the absorption and emission maxima shifted to 364, 261 nm and 479, 372, 326 nm respectively.

While adding BSA to the Ag nano solution, the absorption maxima red shifted to 454, 277 nm and the emission maximum blue shifted to 350 nm respectively. VF/BSA solution added to the Ag nanoparticles, the absorption maxima blue shifted to 401, 256 nm and the emission maxima red shifted to 495, 323 nm respectively. Due to the Ag nanoparticles interaction with VF, PAMAM-OH dendrimer, DNA, RNA, and BSA red or blue shift was noticed in the absorption and emission spectra. Generally, due to interaction tends to increase or decrease the intensity of the drug and biomolecules. The spectral variation indicates to confirm the interaction between VF, biomolecules and Ag nanoparticles.

Molecular Docking of VF with the biomolecules

The computer simulated automated docking studies were performed using the widely distributed molecular docking software **autodock 1.5.6.** In PAMAM-OH, DNA, RNA, and BSA the following protein data bank ID **1bna**, **2ke6, 3vo3,** and **5d2a** were used respectively. Among the various conformers of docking results, only 10 conformers were taken on the basis of the free energy of binding and score ranking. The minimum binding energy conformer is shown in Figs.3 and 4. The image in Fig. 3a and Fig. 3e shows, DNA and RNA present in double stranded helix structure. As shown in Fig. 4a, and Fig.4e, the micro-ribbons formed by BSA and PAMAM dendrimers are dispersed randomly in the aqueous solution and the length of the micro-ribbons is significantly different from their width. The binding energy (ΔG_b, kcal/mol), intermolecular energy (kcal/mol), torsional energy, total internal energy, inhibition constant (Ki, uM), van der Waals + H bond + desolvation energy (kcal/mol), electro static energy (kcal/mol), ligand efficiency, unbound energy, refRMS are calculated and the data are given in Table 2.

In VF drug, the nitrogen, oxygen, chlorine and hydrogen atoms were docked deeply within the grooves and amino acid of the biomolecules and forming more intercalative sensing or hydrogen bonds with the biomolecules. In **PAMAM-OH**, VF drug interacts at PRO112, TRP111, ASN88, ASN85 and PRO9. In **DNA**, VF interacted with nucleotide sites at DA17, DC11, DG10, DG11, DG14, and DG16, while in **RNA**, VF drug interacts the nucleotide sites at A31, A32, A33, U16, U17. In **BSA,** VF drug interacts the amino acids at ARG1150, ASP114, HIS1144, HIS1159, LEU1156, PRO1151, GLU1155 and GLN1149.

The binding energy, intermolecular energy, van der Waals + H bond + desolvation energy, ligand efficiency of VF with DNA is higher than RNA, BSA and PAMAM-OH. The above results suggest that sensing of VF with DNA is higher than other biomolecules. The higher affinity is presumably attributed to the formation of more and/or tighter hydrogen bonds between the several base pairs at the binding site owing to the increased electronegativity of the hydrogen and oxygen. In other words, they possess the highest potential binding affinity into the binding site of the 3D macromolecule.

ISSN No. 2321-2705 | DOI: 10.51244/IJRSI |Volume XIII Issue III March 2026

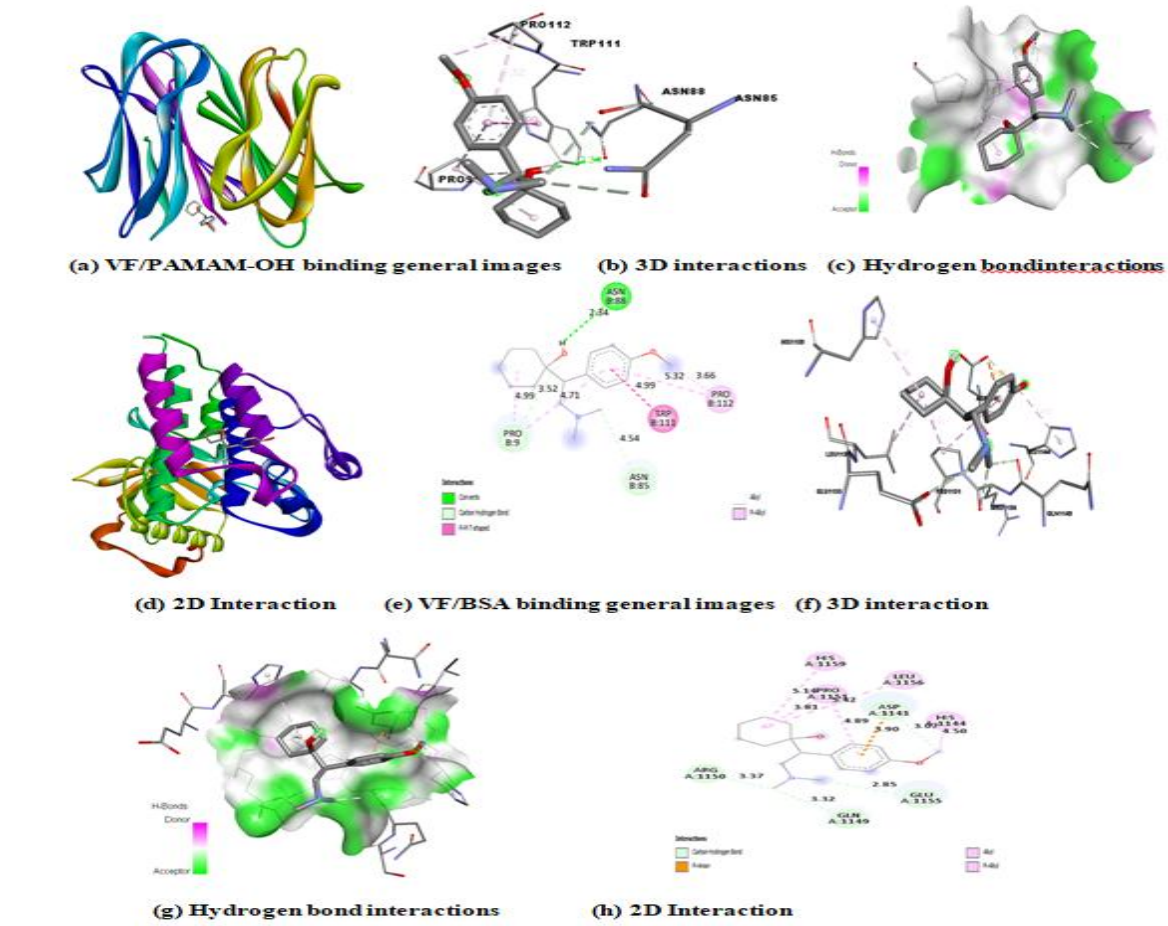

Fig. 3. Venlafaxine HCl with biomolecule interaction images for (a-d) VF/Dendrimer binding image, (e-h) VF/BSA binding images.

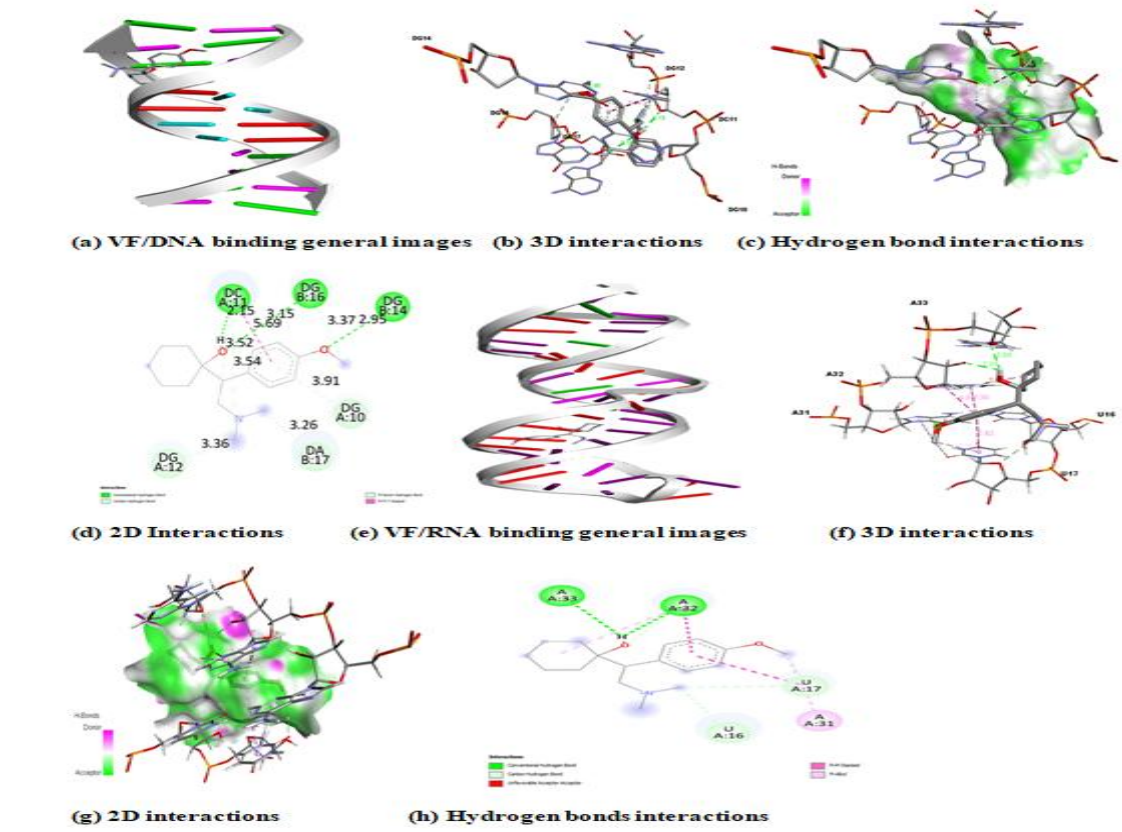

Fig. 4 Venlafaxine HCl with biomolecule interaction images for (a-d) VF/DNA binding image, (e-h) VF/RNA binding images.

ISSN No. 2321-2705 | DOI: 10.51244/IJRSI |Volume XIII Issue III March 2026

Anticancer Potential of Venlafaxine HCl

The anticancer potential of venlafaxine hydrochloride (VF; ID No. 62923) was investigated through molecular docking analyses (Figs. 5 and 6). Figures 5 and 6 illustrate the three-dimensional (3D) and two-dimensional (2D) binding interactions, respectively, between the epidermal growth factor receptor (EGFR) complexed with epiregulin (EREG) (PDB ID: 5WB7) and VF. Detailed docking studies revealed notable interactions between VF and EGFR-associated proteins. With the **1R51 protein**, VF formed three carbon–hydrogen bonds involving Tyr275, Arg273, and Cys272, in addition to four alkyl interactions at Val299, Arg300, Val277, and Lys270. This complex yielded a **LibDock score of 89.29**. Similarly, docking with the **2oh4** protein revealed π-alkyl interactions at Phe1045, Ala1063, and Ile1051, with a higher **LibDock** score of **100.78,** indicating a stronger binding affinity.

To complement the docking analysis, the pharmacokinetic and toxicological properties of VF were predicted using the AutoDock and ADMET platforms. The compound demonstrated a moderate solubility level is **3**, limited blood-brain barrier (BBB) penetration is **1**, and an extended hepatotoxicity model (EXT Hepatotoxic MD) score of approximately **11.47**. VF was predicted not to inhibit CYP2D6, but showed a positive prediction for hepatotoxicity. The plasma protein binding (PPB) prediction was negative, suggesting a lower likelihood of extensive binding to plasma proteins.

The PPB data, particularly in the context of siRNA co-administration, reflect the unbound drug fraction (fu) under equilibrium conditions a critical determinant of pharmacological activity as per the free drug hypothesis, which posits that only the unbound drug is capable of exerting therapeutic effects at the target site during steady-state conditions. Thus, VF exhibits favorable binding interactions with both 1r51 and 2oh4 EGFR targets and displays a pharmacokinetic profile that supports further investigation into its potential as an anticancer agent.

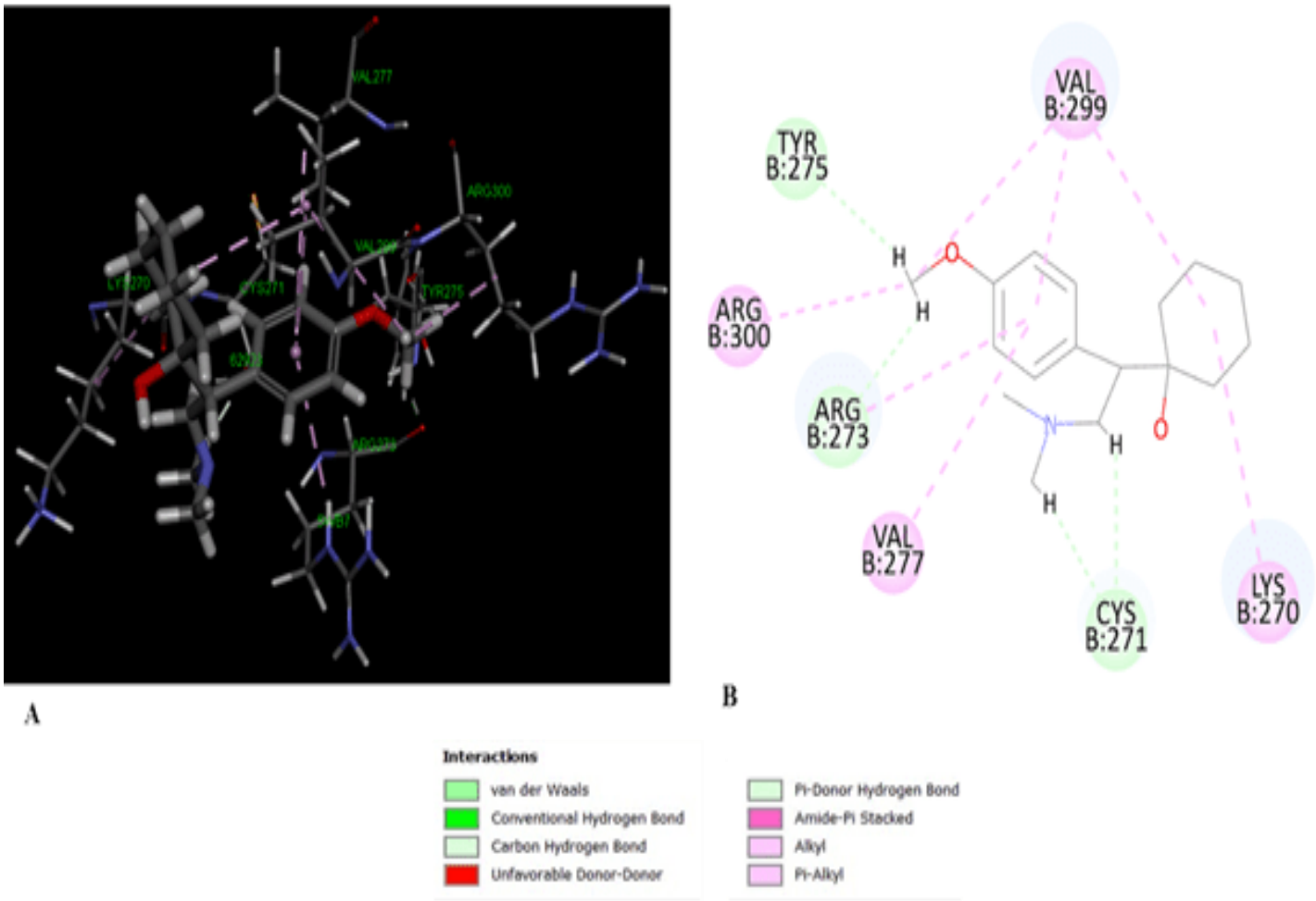

Fig.5. Anticancer potential of venlafaxine HCl with 1r51 protein

ISSN No. 2321-2705 | DOI: 10.51244/IJRSI |Volume XIII Issue III March 2026

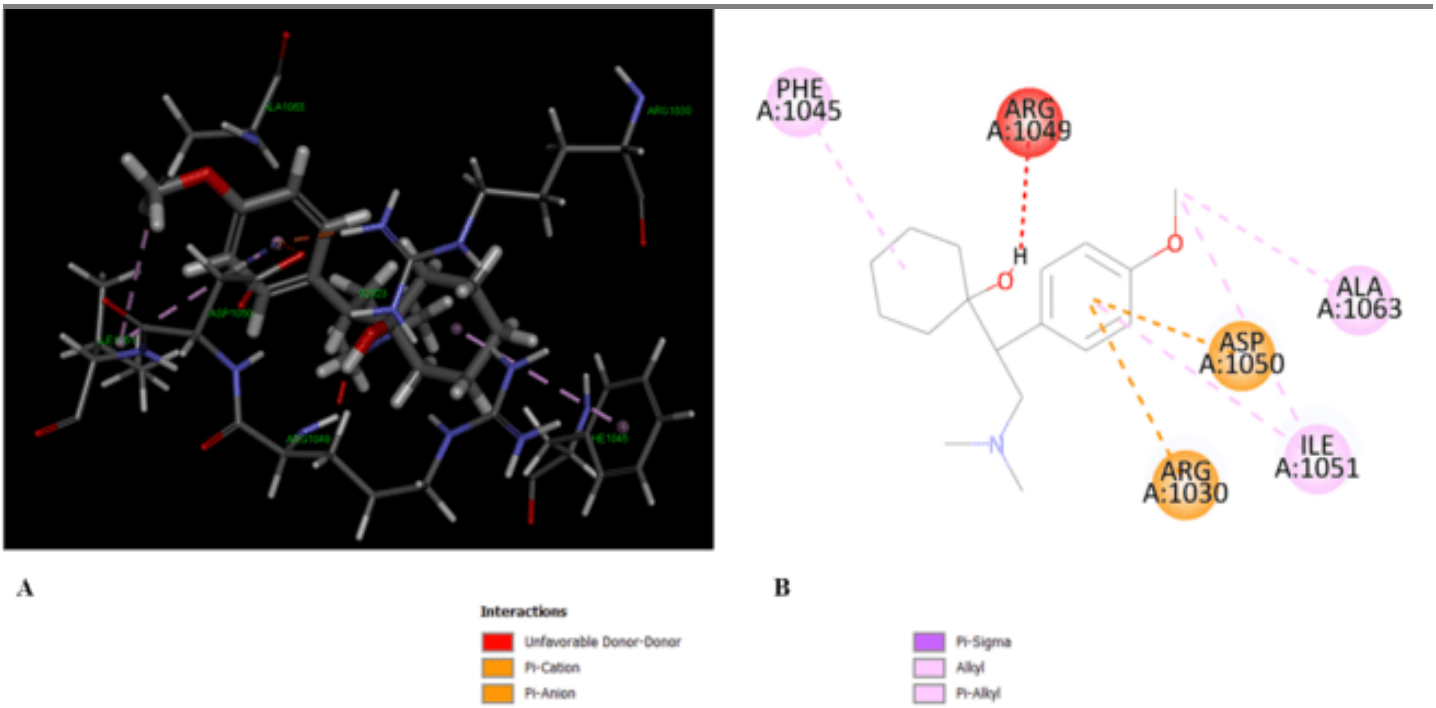

Fig.6. Anticancer potential of venlafaxine HCl with 2oh4 protein

CONCLUSION

Absorption, emission and molecular docking characteristics of venlafaxine HCl (VF) drug with PAMAM-OH, DNA, RNA and BSA silver nanoparticles were analysed. With addition of VF, the absorption and emission maxima of the biomolecules are completely disappeared. When biomolecule concentrations increased, the absorption and emission intensities of the VF drug was gradually increased or decreased. The negative ΔG^0 values indicate that the spontaneity of the binding between the drugs and biomolecules. The binding affinity of drug to DNA is higher in the ground state, while RNA is higher in the excited state. The intercalative binding, van der Waals force and hydrogen bonding play major roles in the sensing of the drugs and biomolecules. With an addition of VF/biomolecules to the Ag nanoparticles, the absorption and emission maxima were red or blue shifted. Molecular docking results indicated that the biomolecules interacted with the N, O and H group of the VF drug and VF demonstrates promising anticancer activity through interactions with both the 1r51 and 2oh4 EGFR protein targets.

ACKNOWLEDGEMENT

This work was supported by the RUSA PHASE -2.0 [No. 128/A1/ RUSA 2.0, Health and Environment] New Delhi, India. One of the authors, A.Mani is thankful to the RUSA, New Delhi, India for the award of JRF fellowship.

Declaration of Competing Interest

The authors declare no conflict of interest.

REFERENCES

1. N. Shivakumar, P.M. Krishna, Synthesis, spectral characterization and DNA interactions of 5-(4-substituted phenyl)-1,3,4-thiadiazol-2-amine scaffolds, *J. Mol. Struct.* **1199** (2020) 126999–127008. https://doi.org/10.1016/j.molstruc.2019.126999
2. R.Y. Sathe, P.V. Bharatam, Drug–dendrimer complexes and conjugates: Detailed furtherance through theory and experiments, *Adv. Colloid Interface Sci.* **303** (2022) 102639–102660. https://doi.org/10.1016/j.cis.2022.102639

3. D. Rout, S. Sharma, P. Agarwala, A.K. Upadhyaya, A. Sharma, Interaction of ibuprofen with partially unfolded bovine serum albumin in the presence of ionic micelles and oligosaccharides at different λ_ex and pH: A spectroscopic analysis, *ACS Omega* **8** (2023) 3114–3128. https://doi.org/10.1021/acsomega.2c06447
4. H. Monirinasab, M. Zakariazadeh, H. Kohestani, M. Kouhestani, F. Fathi, Study of β-lactam-based drug interaction with albumin protein using optical, sensing, and docking methods, *J. Biol. Phys.* **48** (2022) 177–194. https://doi.org/10.1007/s10867-021-09599-0
5. R.N. El Gammal, H. Elmansi, A.A. El-Emam, F. Belal, P.A. Elzahhar, A.S.F. Belal, M.E.A. Hammouda, Insights on the in-vitro binding interaction between donepezil and bovine serum albumin, *BMC Chem.* **17** (2023) 1–11. https://doi.org/10.1186/s13065-023-00944-z
6. J. Wang, B. Li, L. Qiu, X. Qiao, H. Yang, Dendrimer-based drug delivery systems: history, challenges, and latest developments, *J. Biol. Eng.* **16** (2022) 1–12. https://doi.org/10.1186/s13036-022-00298-5
7. R.V. Araujo, S.S. Santos, E.I. Ferreira, J. Giarolla, New advances in general biomedical applications of PAMAM dendrimers, *Molecules* **23** (2018) 1–27. https://doi.org/10.3390/molecules23112849
8. D. Maciel, C. Guerrero-Beltran, R. Cena-Diez, H. Tomas, M.A. Munoz-Fernandez, J.M. Rodrigues, New anionic poly(alkylid:namine) dendrimers as microbicide agents against HIV-1 infection, *Nanoscale* **11** (2019) 9679–9690. https://doi.org/10.1039/C9NR00303G
9. D.E. Igartua, C.S. Martinez, S.V. Alonso, M.J. Prieto, Combined therapy for Alzheimer's disease: Tacrine and PAMAM dendrimers co-administration reduces the side effects of the drug without modifying its activity, *AAPS PharmSciTech* **21** (2020) 110–124. https://doi.org/10.1208/s12249-020-01652-w
10. G. Helena, J. Roman, Self-assembled bionanostructures: proteins following the lead of DNA nanostructures, *J. Nanobiotechnol.* **12** (2014) 4. https://doi.org/10.1186/1477-3155-12-4
11. D.B. Kokh, L. Calzolai, R.C. Wade, S. Corni, Docking of ubiquitin to gold nanoparticles, *ACS Nano* **6** (2012) 9863–9878. https://doi.org/10.1021/nn303444b
12. A. Vila Verde, J.M. Acres, J.K. Maranas, Investigating the specificity of peptide adsorption on gold using molecular dynamics simulations, *Biomacromolecules* **10** (2009) 2118–2128. https://doi.org/10.1021/bm9002464
13. L.A. Dykman, N.G. Khlebtsov, Gold nanoparticles in biology and medicine: Recent advances and prospects, *Acta Nat.* **3** (2011) 34–55. https://doi.org/10.32607/20758251-2011-3-2-34-55
14. U.K. Parida, P.L. Nayak, Biomedical applications of gold nanoparticles, *World J. Nucl. Sci. Technol.* **1** (2012) 10–25. https://doi.org/10.1155/2013/123838
15. M. Rahman, S. Laurent, N. Tawil, L. Yahia, M. Mahmoudi, Protein–nanoparticle interactions, Springer-Verlag, Berlin, Heidelberg, 2013. https://doi.org/10.1007/978-3-642-37555-2
16. S.R. Saptarshi, A. Duschl, A.L. Lopata, Interaction of nanoparticles with proteins: relation to bioreactivity of the nanoparticle, *J. Nanobiotechnol.* **11** (2013) 26. https://doi.org/10.1186/1477-3155-11-26
17. D.H. Tsai, F.W. Delrio, A.M. Keene, K.M. Tyner, R.I. Maccuspie, T.J. Cho, M.R. Zachariah, V.A. Hackley, Adsorption and conformation of serum albumin protein on gold nanoparticles investigated using dimensional measurements and in situ spectroscopic methods, *Langmuir* **27** (2011) 2464–2477. https://doi.org/10.1021/la104124d
18. F. Ramezani, H. Rafii-Tabar, An in-depth view of human serum albumin corona on gold nanoparticles, *Mol. BioSyst.* (2014) 1–9. https://doi.org/10.1039/c4mb00591k
19. A. Mani, P. Ramasamy, A. Antony Muthu Prabhu, N. Rajendiran, Investigation of Ag and Ag/Co bimetallic nanoparticles with naproxen–cyclodextrin inclusion complex, *J. Mol. Struct.* **1284** (2023) 135301–135310. https://doi.org/10.1016/j.molstruc.2023.135301
20. A. Mani, G. Venkatesh, P. Senthilraja, N. Rajendiran, Synthesis and characterisation of Ag–Co–venlafaxine–cyclodextrin nanorods, *Eur. J. Adv. Chem. Res.* **5** (2024) 9–16. https://doi.org/10.24018/ejchem.2024.5.1.147
21. A. Mani, P. Ramasamy, A. Antony Muthu Prabhu, P. Senthilraja, N. Rajendiran, Synthesis and analysis of Ag/olanzapine/cyclodextrin and Ag/Co/olanzapine/cyclodextrin inclusion complex nanorods, *Phys. Chem. Liq.* **62** (2024) 196–209. https://doi.org/10.1080/00319104.2023.2297223

22. A. Mani, P. Ramasamy, A. Antony Muthu Prabhu, P. Senthilraja, N. Rajendiran, Synthesis and characterisation of Ag/Co/chloroquine/cyclodextrin inclusion complex nanomaterials, *J. Sol–Gel Sci. Technol.* **115** (2025) 844–856. https://doi.org/10.1007/s10971-024-06620-5
23. G.M. Morris, D.S. Goodsell, R.S. Halliday, R. Huey, W.E. Hart, R.K. Belew, A.J. Olson, Automated docking using a Lamarckian genetic algorithm and an empirical binding free energy function, *J. Comput. Chem.* **19** (1998) 1639–1662. https://doi.org/10.1002/(SICI)1096-987X(19981115)19:14<1639::AID-JCC10>3.0.CO;2-B
24. R. Huey, G.M. Morris, A.J. Olson, D.S. Goodsell, A semiempirical free energy force field with charge-based desolvation, *J. Comput. Chem.* **28** (2007) 1145–1152. https://doi.org/10.1002/jcc.20634
25. G.M. Morris, M. Lim-Wilby, Molecular docking, in: A. Kukol (Ed.), *Molecular Modeling of Proteins, Methods in Molecular Biology*, vol. 443, Humana Press, Totowa, NJ, 2008, pp. 365–382. https://doi.org/10.1007/978-1-59745-177-2_19
26. O. Trott, A.J. Olson, AutoDock Vina: improving the speed and accuracy of docking with a new scoring function, efficient optimization, and multithreading, *J. Comput. Chem.* **31** (2010) 455–461. https://doi.org/10.1002/jcc.21334
27. A.D. Hill, P.J. Reilly, Scoring functions for AutoDock, in: *Methods in Molecular Biology*, vol. 1273, Springer, New York, 2015, pp. 467–474. https://doi.org/10.1007/978-1-4939-2343-4_27
28. T.A. Halgren, Merck molecular force field. I. Basis, form, scope, parameterization, and performance of MMFF94, *J. Comput. Chem.* **17** (1996) 490–519. https://doi.org/10.1002/(SICI)1096-987X(199604)17:5/6<490::AID-JCC1>3.0.CO;2-P
29. N. Rajendiran, J. Thulasidhasan, Interaction of sulfanilamide and sulfamethoxazole with bovine serum albumin and adenine: spectroscopic and molecular docking investigations, Spectrochim. Acta A Mol. Biomol. Spectrosc. 144 (2015) 183–191. https://doi.org/10.1016/j.saa.2015.01.127
30. N. Rajendiran, J. Thulasidhasan, Study of the binding of thiazolyazoresorcinol and thiazolyazocresol dyes with BSA and adenine by spectral, electrochemical and molecular docking methods, Can. Chem. Trans. 3 (2015) 291–307. https://doi.org/10.13179/canchemtrans.2015.03.03.0209
31. N. Rajendiran, J. Thulasidhasan, Binding of sulfamerazine and sulfamethazine to bovine serum albumin and nitrogen purine base adenine: a comparative study, Int. Lett. Chem. Phys. Astron. 59 (2015) 170–187. https://doi.org/10.18052/www.scipress.com/ILCPA.59.170
32. N. Rajendiran, J. Thulasidhasan, Spectral, electrochemical and molecular docking studies on the interaction of dothiepin and doxepin with BSA and DNA base, Luminescence 31 (2016) 1438–1447. https://doi.org/10.1002/bio.3126
33. N. Rajendiran, J. Thulasidhasan, Effects of interaction between non-steroidal anti-inflammatory drugs with BSA and DNA base: spectral, electrochemical and molecular docking methods, J. Indian Chem. Soc. 94 (2017) 83–93.
34. N. Rajendiran, J. Thulasidhasan, M. Suresh, Investigation on the interaction of sulfonyl derivatives with BSA and DNA base by spectral and molecular docking analysis, Arch. Appl. Sci. Res. 9 (2017) 11–18.
35. N. Rajendiran, M. Suresh, Spectroscopic, electrochemical and molecular docking studies on the biosensing of ofloxacin, norfloxacin with different biomolecules, Int. J. Chem. Pharm. Sci. 8 (2017) 1–18.
36. N. Rajendiran, J. Thulasidhasan, M. Suresh, Interaction of azo dyes with BSA and adenine: spectral, electrochemical and molecular docking methods, Der Pharma Chemica 10 (2018) 50–66.
37. J. Thulasidhasan, R. Anandhi, G.V. Kumar, N. Rajendiran, Interaction of Fast Garnet GBC with bovine serum albumin: spectral, electrochemical and molecular docking methods, Int. J. Innov. Res. Stud. 8 (2018) 111–119.
38. N. Rajendiran, M. Suresh, Study of the interaction of ciprofloxacin and sparfloxacin with biomolecules by spectral, electrochemical and molecular docking methods, Int. Lett. Chem. Phys. Astron. 78 (2018) 1–29. https://doi.org/10.18052/www.scipress.com/ILCPA.78.1
39. J. Liu, T. Zhang, T. Lu, L. Qu, H. Zhou, Q. Zhang, L. Ji, DNA-binding and cleavage studies of macrocyclic copper(II) complexes, J. Inorg. Biochem. 91 (2002) 269–276. https://doi.org/10.1016/S0162-0134(02)00441-5
40. M. Sirajuddin, S. Ali, A. Haider, N.A. Shah, A. Shah, M.R. Khan, Synthesis, characterization, biological screenings and interaction with calf thymus DNA as well as electrochemical studies of

adducts formed by azomethine [2-((3,5-dimethylphenylimino)methyl)phenol] and organotin(IV) chlorides, Polyhedron 40 (2012) 19–31. https://doi.org/10.1016/j.poly.2012.03.048

41. M. Sirajuddin, S. Ali, N.A. Shah, M.R. Khan, M.N. Tahir, Synthesis, characterization, biological screenings and interaction with calf thymus DNA of a novel azomethine 3-((3,5-dimethylphenylimino)methyl)benzene-1,2-diol, Spectrochim. Acta A Mol. Biomol. Spectrosc. 94 (2012) 134–142. https://doi.org/10.1016/j.saa.2012.03.068
42. F. Arjmand, A. Jamsheera, DNA binding studies of new valine derived chiral complexes of tin(IV) and zirconium(IV), Spectrochim. Acta A Mol. Biomol. Spectrosc. 78 (2011) 45–51. https://doi.org/10.1016/j.saa.2010.06.009
43. G. Pratviel, J. Bernadou, B. Meunier, DNA and RNA cleavage by metal complexes, Adv. Inorg. Chem. 45 (1998) 251–300. https://doi.org/10.1016/S0898-8838(08)60027-6
44. N. Shahabadi, S. Kashanian, M. Khosravi, M. Mahdavi, Multi-spectroscopic DNA interaction studies of a water-soluble nickel(II) complex containing different dinitrogen aromatic ligands, Transit. Met. Chem. 35 (2010) 699–705. https://doi.org/10.1007/s11243-010-9382-x
45. K.A. Kumar, K.L. Reddy, S. Vidhisha, S. Satyanarayana, Synthesis, characterization and DNA binding and photocleavage studies of $[Ru(bpy)_2BDPPZ]^{2+}$, $[Ru(dmb)_2BDPPZ]^{2+}$ and $[Ru(phen)_2BDPPZ]^{2+}$ complexes and their antimicrobial activity, Appl. Organomet. Chem. 23 (2009) 409–420. https://doi.org/10.1002/aoc.1534
46. A. Shah, M. Zaheer, R. Qureshi, Z. Akhter, M.F. Nazar, Voltammetric and spectroscopic investigations of 4-nitrophenylferrocene interacting with DNA, Spectrochim. Acta A Mol. Biomol. Spectrosc. 75 (2010) 1082–1087. https://doi.org/10.1016/j.saa.2009.12.061
47. A. Slistan-Grijalva, R. Herrera-Urbina, J. Rivas-Silva, M. Ávalos-Borja, F. Castillón-Barraza, A. Posada-Amarillas, Classical theoretical characterization of the surface plasmon absorption band for silver spherical nanoparticles suspended in water and ethylene glycol, Physica E Low-Dimens. Syst. Nanostruct. 27 (2005) 104–112. https://doi.org/10.1016/j.physe.2004.10.014
48. A.M. Fayaz, K. Balaji, M. Girilal, P. Kalaichelvan, R. Venkatesan, Mycobased synthesis of silver nanoparticles and their incorporation into sodium alginate films for vegetable and fruit preservation, J. Agric. Food Chem. 57 (2009) 6246–6252. https://doi.org/10.1021/jf900337h
49. M. Sastry, K.S. Mayya, K. Bondyopadhyay, pH dependent changes in the optical properties of carboxylic acid derivatized silver colloidal particles, Colloids Surf. A Physicochem. Eng. Asp. 127 (1997) 221–228. https://doi.org/10.1016/S0927-7757(97)00087-3
50. S. Wu, C. Yang, F. Tsao, P. Huang, M. Chung, W.H. Li, Tunneling magnetoresistance in Ag/Co nanoparticle composites, J. Magn. Magn. Mater. 294 (2005) e83–e86. https://doi.org/10.1016/j.jmmm.2005.03.059
51. H. Wang, X. Qiao, J. Chen, S. Ding, Preparation of silver nanoparticles by chemical reduction method, Colloids Surf. A Physicochem. Eng. Asp. 256 (2005) 111–115. https://doi.org/10.1016/j.colsurfa.2004.12.058
52. J. Garcia-Torres, E. Vallés, E. Gómez, Synthesis and characterization of Co@Ag core–shell nanoparticles, J. Nanopart. Res. 12 (2010) 2189–2199. https://doi.org/10.1007/s11051-009-9784-x
53. N.S. Sobal, M. Hilgendorff, H. Moehwald, M. Giersig, M. Spasova, T. Radetic, M. Farle, Synthesis and structure of colloidal bimetallic nanocrystals: the non-alloying system Ag/Co, Nano Lett. 2 (2002) 621–624. https://doi.org/10.1021/nl025533f